1997

Analysis of the effects of dynamic characteristic dimension calculations on FLIR performance prediction models.

Eaton, Jeffery P.

Monterey, California. Naval Postgraduate School

NAVAL POSTGRADUATE SCHOOL
MONTEREY, CALIFORNIA

THESIS

ANALYSIS OF THE EFFECTS OF DYNAMIC CHARACTERISTIC DIMENSION CALCULATIONS ON FLIR PERFORMANCE PREDICTION MODELS

by

Jeffery P. Eaton

March, 1997

Thesis Advisor: Kneale T. Marshall

Approved for public release; distribution is unlimited.

REPORT DOCUMENTATION PAGE

Form Approved OMB No. 0704-0188

1. AGENCY USE ONLY *(Leave blank)*	2. REPORT DATE March 1997	3. REPORT TYPE AND DATES COVERED Master's Thesis

4. TITLE AND SUBTITLE Analysis of the Effects of Dynamic Characteristic Dimension Calculations on FLIR Performance Prediction Models

5. FUNDING NUMBERS

6. AUTHOR(S) Jeffery P. Eaton

7. PERFORMING ORGANIZATION NAME(S) AND ADDRESS(ES)
Naval Postgraduate School
Monterey CA 93943-5000

8. PERFORMING ORGANIZATION REPORT NUMBER

9. SPONSORING/MONITORING AGENCY NAME(S) AND ADDRESS(ES)

10. SPONSORING/MONITORING AGENCY REPORT NUMBER

11. SUPPLEMENTARY NOTES The views expressed in this thesis are those of the author and do not reflect the official policy or position of the Department of Defense or the U.S. Government.

12a. DISTRIBUTION/AVAILABILITY STATEMENT
Approved for public release; distribution is unlimited.

12b. DISTRIBUTION CODE

13. ABSTRACT *(maximum 200 words)*

The ability to accurately predict the performance of FLIR systems has become critical to today's military. The current U.S. defense industry standard FLIR analysis model is FLIR92 by the U.S. Army's C2NVEO. The algorithm in FLIR92 for calculating target acquisition probabilities, called ACQUIRE, has several limitations in its design for calculating a target's characteristic dimension.

This thesis develops a Dynamic Model to overcome these limitations. It incorporates a three dimensional view of a target based on range, azimuth angle to target, and the altitude of the FLIR sensor. An analysis of the effects of dynamically calculating a target's characteristic dimension by the Dynamic Model and the static ACQUIRE version 1 model is presented. Both are compared on a theoretical target from three different angles; the front, the 45, and the side, with the Dynamic Model producing an 8% increase in prediction ranges for the front, a 4% increase for the 45° view, and a 5% increase for the side. An Empirical Cumulative Tail Distribution is computed from experimental data, and the theoretical probability vs. range predictions of each model are then compared to actual observations. A sensitivity analysis is performed to demonstrate the effects of various conditions on predicted acquisition ranges.

14. SUBJECT TERMS Thermal Imaging, Forward Looking Infrared, FLIR, Infrared, Dynamic Analysis, FLIR Performance Prediction, Characteristic Dimension, Transmissivity, Probability of Detection.

15. NUMBER OF PAGES 72

16. PRICE CODE

17. SECURITY CLASSIFICATION OF REPORT	18. SECURITY CLASSIFICATION OF THIS PAGE	19. SECURITY CLASSIFICATION OF ABSTRACT	20. LIMITATION OF ABSTRACT
Unclassified	Unclassified	Unclassified	UL

NSN 7540-01-280-5500

Standard Form 298 (Rev. 2-89)
Prescribed by ANSI Std. 239-18 298-102

Approved for public release; distribution is unlimited.

ANALYSIS OF THE EFFECTS OF DYNAMIC CHARACTERISTIC DIMENSION CALCULATIONS ON FLIR PERFORMANCE PREDICTION MODELS

Jeffery P. Eaton
Lieutenant, United States Navy
B.S., Florida State University, 1987

Submitted in partial fulfillment
of the requirements for the degree of

MASTER OF SCIENCE IN OPERATIONS RESEARCH

from the

NAVAL POSTGRADUATE SCHOOL
March 1997

Author: [redacted]
Jeffery P. Eaton

Approved by: [redacted]
Kneale T. Marshall, Thesis Advisor

[redacted]
Gordon Bradley, Second Reader

[redacted]
Frank C. Petho, Chairman
Department of Operations Research

ABSTRACT

The ability to accurately predict the performance of FLIR systems has become critical to today's military. The current U.S. defense industry standard FLIR analysis model is FLIR92 by the U.S. Army's C2NVEO. The algorithm in FLIR92 for calculating target acquisition probabilities, called ACQUIRE, has several limitations in its design for calculating a target's characteristic dimension.

This thesis develops a Dynamic Model to overcome these limitations. It incorporates a three dimensional view of a target based on range, azimuth angle to target, and the altitude of the FLIR sensor. An analysis of the effects of dynamically calculating a target's characteristic dimension by the Dynamic Model and the static ACQUIRE version 1 model is presented. Both are compared on a theoretical target from three different angles; the front, the 45, and the side, with the Dynamic Model producing an 8% increase in prediction ranges for the front, a 4% increase for the 45° view, and a 5% increase for the side. An Empirical Cumulative Tail Distribution is computed from experimental data, and the theoretical probability vs. range predictions of each model are then compared to actual observations. A sensitivity analysis is performed to demonstrate the effects of various conditions on predicted acquisition ranges.

TABLE OF CONTENTS

EXECUTIVE SUMMARY

Infrared imaging is an industry that has widespread applications in both the military and civilian communities. Since the 1960's, Forward Looking Infrared, or FLIR, has undergone dramatic changes, both technologically and in its applications. The military, since 1980, has implemented FLIR into virtually all high value platforms. This investment has produced a large industrial community dedicated not only to the manufacture of FLIR systems but also to their integration into weapons, aircraft, vehicles, and ships. As a result, a requirement exists to accurately analyze, measure, and predict the performance of FLIR systems.

The current U.S. defense industry standard FLIR analysis model is comprised of two computer algorithms by the U.S. Army's CECOM Center for Night Vision and Electro-Optics (C2NVEOL). They are FLIR92 and ACQUIRE. FLIR92 is based on the Laboratory's 1975 Static Performance Model and has been updated to predict the performance of first, second, and third generation FLIR systems. ACQUIRE is an analytical model that predicts target acquisition performance for systems that image in the visible, near infrared, and infrared spectral bands. The focus of this thesis is on the calculation of the acquisition probabilities, and therefore is limited in discussion to the ACQUIRE version 1 model, dated May 1995.

In calculating the acquisition probability, selecting a proper measure of the target size is critical to obtain consistent performance predictions. This "target size" is referred to as the target's *characteristic dimension*, based on the area of a target. Unfortunately, ACQUIRE has several weaknesses in this area, and is inadequate when used in any scenario other than land combat.

This thesis develops a Dynamic Model to overcome these limitations. It incorporates a three dimensional view of a target based on range, the azimuth angle to the target, and the altitude of the FLIR sensor. An analysis of the effects of dynamically calculating a target's

characteristic dimension by the Dynamic Model and the static ACQUIRE version 1 model is presented. Both models are compared on a theoretical target from three different angles; the front, the 45, and the side, with the Dynamic Model producing an 8% increase in prediction ranges for the front, a 4% increase for the 45° view, and a 5% increase for the side. An Empirical Cumulative Tail Distribution is computed from experimental data, and the theoretical probability vs. range predictions of each model are then compared to actual observations. Despite the small sample size from the experiment, both models' predictions compare favorably against the actual detection ranges. For the front view, the Dynamic Model provides 4% longer prediction ranges, a closer representation of the empirical distribution. A sensitivity analysis is then performed to demonstrate the effects of various conditions on predicted acquisition ranges.

I. INTRODUCTION

A. GENERAL

Infrared imaging is an industry that has widespread applications in both the military and civilian communities. Since the 1960's, Forward Looking Infrared, or FLIR, has undergone dramatic changes, both technologically and in its applications. The military, since 1980, has implemented FLIR into virtually all high value platforms. This investment has produced a large industrial community dedicated not only to the manufacture of FLIR systems but also to their integration into weapons, aircraft, vehicles, and ships [Ref. 5: p. 1-1]. As a result, a requirement exists to accurately analyze, measure, and predict the performance of FLIR systems.

In order to predict the performance of FLIR systems, it is essential for a model to calculate the system's summary performance measures of Minimum Resolvable Temperature Difference (MRTD) or Minimum Detectable Temperature Difference (MDTD) between a target and its background, and to calculate the acquisition probabilities for a particular scenario. The accuracy of these calculations will ultimately determine the accuracy of the model by which the FLIR system's performance is evaluated.

The current U.S. defense industry standard FLIR analysis model is comprised of two computer algorithms by the U.S. Army's CECOM Center for Night Vision and Electro-Optics (C2NVEOL) [Ref 4: p. 218]. They are FLIR92 and ACQUIRE. FLIR92 is based on the Laboratory's 1975 Static Performance Model and has been updated to predict the performance of first, second, and third generation FLIR systems [Ref. 2: p. 1]. It calculates the system's summary performance measure, MRTD or MDTD. ACQUIRE is an analytical model that predicts target acquisition performance for systems that image in the visible, near infrared, and infrared spectral bands. The two algorithms can be run sequentially, or if the

system MRTD/MDTD is already known through laboratory measurements, then ACQUIRE can be run alone. The focus of this thesis is on the calculation of the acquisition probabilities, and therefore is limited in discussion to the ACQUIRE version 1 model, dated May 1995.

In calculating the acquisition probability, selecting a proper measure of the target size is critical to obtain consistent performance predictions. This "target size" is referred to as the target's *characteristic dimension*, based on the area of a target. Unfortunately, ACQUIRE has several weaknesses in this area. It depends upon: (1) a look up table that consists of only a limited set of military land vehicles, (2) having the user input only the target's height and length, or, (3) making off-line calculations in order to input the target's characteristic dimension. These off-line calculations require that the user make a "best guess" at the predicted range and then calculate the characteristic dimension for that range. This often results in the model having to be run multiple times in order to accurately predict the FLIR performance. If a target is not in the look up table, this becomes a very time consuming and cumbersome process. Another limitation in the ACQUIRE model is that the FORTRAN code uses only the target's length and height for the target's characteristic dimension calculations, and once calculated, this value does not change. This serves to give only a two dimensional view of the target and does not account for the changing target area associated with changes in range and azimuth. When calculating such things as projected target area, a three dimensional representation of a target will be much more accurate in predicting FLIR system performance. These factors all combine to make the ACQUIRE model inadequate when used in any scenario other than land combat.

B. STATEMENT OF THESIS

This thesis examines these inadequacies and develops a Dynamic Model that incorporates a three dimensional view of a target for the characteristic dimension

calculations. This accounts for changes in the target's area based on range, the azimuth angle to the target, and the altitude of the FLIR sensor. The Dynamic Model is implemented in PASCAL code, contained in Appendix A. An analysis is then performed to determine the effects of the dynamically calculated characteristic dimension vs. the static predictions of the ACQUIRE version 1 model. A simulation of each model is run using the AN/AAS-36 FLIR system parameters and using the Research Vessel *POINT SUR* as the target. The theoretical probability vs. range predictions of each model are then compared to actual observations gained from a P-3 maritime patrol aircraft (MPA) equipped with the AN/AAS-36 FLIR system against the research vessel R/V *POINT SUR*. A sensitivity analysis is then performed on the Dynamic Model to determine how various conditions affect the model's predictions.

II. FLIR THEORY AND CONCEPTS

A. FUNDAMENTALS OF THERMAL IMAGING

The basic elements of any thermal imaging problem are described in the sequential blocks of Figure 2.1 [Ref. 1: p. 7]. To be detected, and subsequently recognized and identified, an object must produce an object-to-background apparent temperature difference large enough to be distinguished from other variations in the background. The intervening atmosphere must not excessively blur or attenuate this signal. The operator then must use an effective search procedure, know what to look for, and point the sensor in the correct direction.

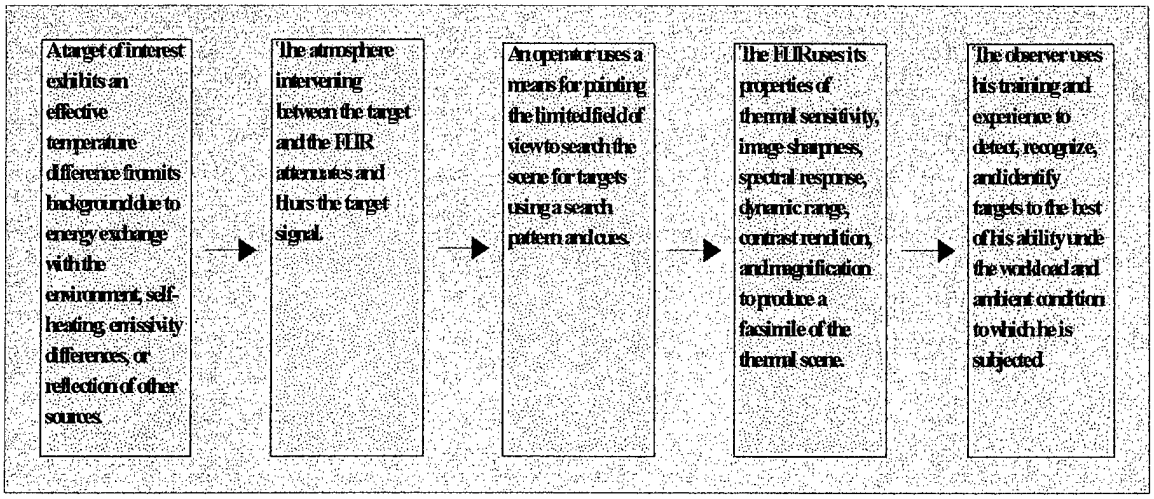

Figure 2.1: Sequence of Events in a Thermal Imaging Process [Ref. 1: p. 7].

The sensor must collect the radiant signal with an optical device, and convert it to an electrical signal with good signal-to-noise ratio in a detector operating in a given spectral band. This electrical signal must then be reconverted to an optical signal on a video display.

Finally, the operator must be able to visually extract information by using video gain and brightness controls. This entire process of converting an infrared scene to an analog visual scene must be performed so that contours, orientations, contrasts, and details are preserved or enhanced, and without introducing artifacts and excessive noise [Ref. 1: p. 6]. The goal is to learn something about a specific object or target. A Thermal Imaging System is used to achieve this goal by extending our vision beyond the visible red and into the far infrared by making use of the radiation naturally emitted by warm objects.

B. INFRARED RADIATION

There are many different types of radiation and all are similar in nature. These can be grouped under a single classification called electromagnetic radiation. These radiations are commonly described by their position in the electromagnetic spectrum, which arranges the various radiations by wavelength or frequency. Wavelengths and frequency are related by the equation:

$$\lambda v = c \tag{2.1}$$

where

- λ is the wavelength of electromagnetic wave (meters),
- v is the frequency of electromagnetic wave (Hz),
- c is the speed of light (3×10^8 meters/second).

The part of the spectrum that includes infrared, has wavelength ranging from 0.75×10^{-6} meters to 1.00×10^{-3} meters, with a corresponding frequency range of 4.00×10^{4} Hz to 3.00×10^{11} Hz . It is bounded on the short-wavelength side by visible light and on the long-wavelength side by microwaves [Ref. 6: p. 20-23]. It is customary to use the micron

(μ) or micrometer (μm), as the unit of wavelength in the infrared. Occasionally the millimicron (mμ), the nanometer (nm), or the angstrom (A) may be encountered as units for wavelength. These are related as follows:

$$1\mu = 10^{-4}\text{cm} = 10^{-6}\text{m},$$

$$1\mu = 10^{3}\ \text{m}\mu = 10^{3}\ \text{nm} = 10^{4}\text{A}.$$

Band Name	Frequency	Wavelength
Near Infrared	395 - 100 T Hz[1]	0.75 - 3 μm
Middle Infrared	100 - 50 T Hz	3 - 6 μm
Far Infrared	50 - 20 T Hz	6 - 15 μm
Extreme Infrared	20 T Hz - 300 G Hz	15 - 1000 μm

Table 2.1 : Subdivisions of the Infrared Spectrum.

Table 2.1 contains the subdivisions of the infrared spectrum [Ref. 4: p. 16]. All of the infrared radiations obey similar laws of reflection, refraction, diffraction, and polarization. The velocity of propagation is the same for all, the speed of light; they differ only in wavelength and frequency [Ref. 6: p. 20].

C. INFRARED SOURCE AND BLACKBODY EMISSION

All objects above an absolute temperature of 0° Kelvin (K) are continually emitting radiation at a rate and with a wavelength distribution that depends on the temperature of the object and its spectral emissivity, ε(λ). The link between visible and infrared systems is in the physics of photons. Photons are generated with a total radiant flux proportional to absolute temperature raised to the fourth power (known as the Stefan-Boltzmann Law) and with a peak energy wavelength inversely proportional to temperature. The differences

[1]Tera-Hertz (10^{12}).

between a visual image and an infrared image is that (1) the visual image is produced primarily by reflection and reflectivity differences and thermal images are produced primarily by self-emission and emissivity differences, and (2) the infrared wavelength is considerably longer than the visual wavelength [Ref. 4: p. 16]. The following thermal radiation laws, equations, and principles are fundamental for Thermal Imaging Systems and were taken from Kreitz [Ref. 7: pp. 9-12] and Dodson [Ref. 9: pp. 4-8]. The equations and notation were verified from Waldman [Ref. 4: pp. 48-52], Hudson [Ref. 6: pp. 33-42], Burnay [Ref. 8: pp. 1-5], and Shumaker [Ref. 5: pp. 2.18 - 2.65].

1. Planck's Blackbody Radiation Law

A blackbody is an object that absorbs all incident radiation and reradiates it uniformly in all directions, the perfect radiator. The energy emitted by a blackbody is the maximum theoretically possible for a given temperature [Ref. 8: p. 1]. The *spectral radiant emittance* of a blackbody is given by Planck's Law, which for convenience is written:

$$W_\lambda = \frac{C_1}{\lambda^5} \frac{1}{e^{\frac{c_2}{\lambda T}} - 1} \tag{2.2}$$

where

W_λ is watts per cm^2 of target area per μm spectral bandwidth,

C_1 is $2\pi c^2 h = 3.7415 \times 10^4$ $Wcm^{-2}\mu m^4$, where h is Planck's constant,

C_2 is $hc/k = 1.4388 \times 10^4$ μm K,

c is the speed of light (3×10^8 meters/second),

k is Boltzmann's constant (1.38054×10^{-23} W sec K^{-1}),

T is the blackbody temperature (K),

λ is wavelength in μm.

Figure 2.2 is a plot of spectral radiant emittance of a blackbody at various temperatures and shows that when spectral radiant emittance increases with temperature, the peak emittance shifts toward shorter wavelengths.

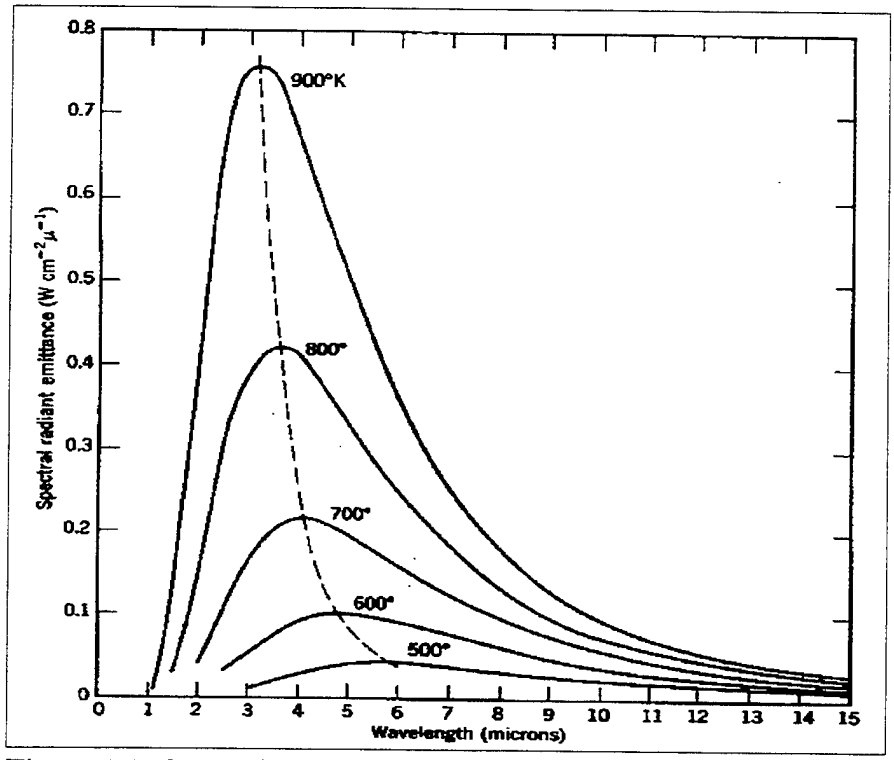

Figure 2.2: Spectral radiant emittance. [Ref. 6: p. 36]

2. Stefan-Boltzmann Law

Integrating Planck's Law, Equation 2.2, over wavelength from zero to infinity gives an expression for the *spectral radiant emittance*, the flux radiated into a hemisphere above a blackbody 1 cm^2 in area [Ref. 6: p. 37]. This is known as the Stefan-Boltzmann Law. This integration, the area under the curve in Figure 2.2, results in:

$$W = \sigma T^4 \tag{2.3}$$

where

W is spectral radiant emittance (Watts/cm^2),

σ is the Stefan-Boltzmann constant (5.6697×10^{-12} Watts/cm^{2}K^4).

This shows the strong dependence of an object's spectral emittance on its temperature.

3. Spectral Emissivity

To determine the radiant emittance of a military target, a non-blackbody source, the *spectral emissivity* is required. Spectral emissivity, $\varepsilon(\lambda)$, is the ratio of the spectral radiant emittance of the source to that of a blackbody at the same temperature [Ref. 6: p. 39]. The range of values for spectral emissivity is 0.0 to 1.0, where 1.0 is a blackbody. This value may vary with wavelength (referred to as a selective radiator); however, for most infrared applications the spectral emissivity of a source is considered to remain constant over all wavelengths (referred to as a graybody source) [Ref. 6: p. 40].

For opaque surfaces, spectral emissivity and reflectivity are related as follows:

$$\varepsilon(\lambda) = 1 - \rho(\lambda) \tag{2.4}$$

where

λ is wavelength,

$\varepsilon(\lambda)$ is the spectral emissivity at wavelength λ,

$\rho(\lambda)$ is the reflectivity at wavelength λ.

4. Lambert-Beer Law

When radiant energy interacts with matter, the energy may be reflected, scattered, or absorbed. Lambert stated that layers of equal thickness absorb equal fractions of the flux

passing through them. For example, if one-half of the flux is absorbed after passing through 1 cm of absorber, passing through a second centimeter will again remove one-half of it, and leave one-fourth of the original flux. He defined the *absorption coefficient* as the reciprocal of the length of the absorbing path necessary to reduce the flux to $1/e$, or 37% of it's initial value [Ref. 6: p. 137]. This absorption coefficient usually varies with wavelength.

Beer noted that the absorption coefficient is proportional to the amount of the absorber in a liquid, or to the pressure in a gas [Ref. 6: p. 137]. The result is the Lambert-Beer Law and is given by:

$$T_a(\lambda) = e^{-\alpha(\lambda)R} \tag{2.5}$$

where

$T_a(\lambda)$ is spectral atmospheric transmittance due to absorption at wavelength λ,

α is the absorption coefficient,

R is the range over which transmittance is desired.

This law is the basis for the calculations to compute the total atmospheric transmittance for a given wavelength in the Dynamic Model. Further discussion on this topic is delayed until Chapter III.

D. TARGET THERMAL SIGNATURE

Most analysis of infrared signatures of targets and their backgrounds is based on the assumption that a target behaves like a blackbody at a temperature some number of degrees different from a uniform blackbody background. Since real targets differ from their backgrounds due to more than just their temperature difference, the temperature difference that is used to characterize targets and their backgrounds for analysis must be calculated to

account for these factors. The resulting "effective" temperature difference, ΔT, is the temperature difference required of two blackbodies to produce the actual in-band average radiance difference between a target and its background [Ref. 5: p. 2.18-2.19]. The value of this ΔT usually depends on the type of target, target history (is it running or has it been moved recently), background, time of day, and local atmospheric conditions. This ΔT, also differs for different FLIR spectral bands. Shumaker [Ref. 5: pp. 2.19-2.66] provides a detailed discussion on all the factors that must be considered in determining the nature and magnitude of thermal signatures, and relates them to a ΔT that can be used to characterize targets for analysis.

E. JOHNSON CRITERIA

In 1958, Johnson conducted an experiment using eight military vehicles and one observer to develop a relationship between spatial frequency and a target. During the experiment, Johnson placed a set of tri-bar patterns next to military targets as he varied conditions. He noted what tri-bar frequency could just be resolved when a given visual discrimination task was accomplished. He then related the visual discrimination levels to the Air Force tri-bar target frequencies using the minimum dimension of the target as a reference.

Discrimination Level	Definition	1-D Cycles Across Minimum Dimension
Detection	An object is present (Object vs. Noise)	1.0 ± 0.25
Orientation	Determining the direction of the long axis (Side view vs. Front view)	1.4 ± 0.35
Recognition	The class to which the object belongs (Tank, Truck, Destroyer)	4.0 ± 0.8
Identification	Determines the specific military designation (T-72 Tank, DD963, CVN69)	6.4 ± 1.5

Table 2.2: Johnson's 1- Dimensional Results.

Table 2.2 contains the discrimination levels, their definitions, and the required one dimension (vertical tri-bar pattern) resolvable cycles across the target's minimum dimension. These cycle criteria provide a 50 % probability of accomplishing the discrimination task.

Through advances in technology and improvements to FLIR systems, Johnson's Criteria have had to be updated. A series of perception tests conducted by the U. S. Army CECOM Center for Night Vision and Electro-Optics (C2NVEO) Visionics Division demonstrated that both horizontal and vertical resolution are equally important to determine the ability of test subjects to perform visual discrimination tasks [Ref. 11: p. 13]. Given this experimental evidence and the acceptance by government and industry, the Johnson cycle criteria have been adjusted. Table 2.3 contains the two dimensional cycle criteria for a 50% probability of task discrimination, that are in current use.

Discrimination Level	Definition	2-D Cycles Across Minimum Dimension
Detection	Same as Above	0.75
Classification	Distinguish Targets from Similar Sized Non-Targets	1.5
Recognition	Same as Above	3.0
Identification	Same as Above	6.0

Table 2.3: Two-Dimensional Johnson Cycle Criteria.

F. TARGET CHARACTERISTIC DIMENSION

In order to establish the bar-chart equivalent of a specific discrimination task, selecting the proper target size is critical in obtaining meaningful results. In Johnson's original work, he chose the *minimum target dimension* as the target's "characteristic dimension ." Johnson, Lawson, and Moser found that using the *average target dimension* (square root of its area) as the "characteristic dimension" led to consistent predictions for targets regardless of aspect, while use of the *minimum dimension* led to erroneous

conclusions [Ref. 5: p. 2.8]. When prior knowledge of the "characteristic dimension" of a target is known, or can be calculated, it should be used in performance predictions. However, when there is no prior target knowledge, the *average dimension* (square root of its area) is recommended for use as the "characteristic dimension," since it is easy to calculate and has led to consistent predictions for both square and elongated targets.

III. COMPETING MODELS

A. STRUCTURE OF A DISCRIMINATION TASK

In a discrimination task, the question to answer is; "At what range can a specific visual task be performed at a given confidence level?" There are basic components to any algorithm that must be determined. They are:

- The target to background temperature differential, ΔT.
- The total atmospheric transmittance, T_A, as a function of range.
- The target's characteristic dimension, D_C, in meters.
- The number of resolvable cycles across that characteristic dimension, N_C.
- The probability of performing the task, given that the target is in the field of view of the sensor and infinite search time is available.

Two FLIR performance prediction models are compared in this thesis, and both are comprised of these components. All formulas are the same in each, except for those used to calculate the target's characteristic dimension. Thus they will only be addressed in Section C, the section containing the Dynamic Model.

B. ACQUIRE VERSION 1 MODEL

The current U.S. defense industry standard FLIR analysis model is comprised of two computer algorithms developed by the U.S. Army's C2NVEO [Ref 4: p. 218]. They are FLIR92 and ACQUIRE. FLIR92 is based on the Laboratory's 1975 Static Performance Model and has been updated to predict the performance of both first, second, and third generation FLIR systems [Ref. 2: p. 1]. The two algorithms can be run sequentially, with

FLIR92 calculating the system's summary performance measures of Minimum Detectable Contrast (MDC), Minimum Detectable Temperature Difference (MDTD), Minimum Resolvable Contrast (MRC), and Minimum Resolvable Temperature Difference (MRTD). These are then used as inputs into ACQUIRE. If these measures are already known, then ACQUIRE can be run alone.

ACQUIRE is an analytical model that predicts target acquisition performance for systems that image in the visible, near infrared, and infrared spectral bands. It can be operated in two modes: target spot detection and target discrimination. Calculations for target spot detection performance are based on Signal to Noise Ratio (SNR) theory and require that the system be characterized by either Minimum Detectable Contrast (MDC) or Minimum Detectable Temperature Difference (MDTD) for model inputs. Calculations for target discrimination performance are based on the two-dimensional Johnson cycle criteria methodology discussed in Chapter II, and require that the system be characterized by either Minimum Resolvable Contrast (MRC) or Minimum Resolvable Temperature Difference (MRTD) for model inputs [Ref. 3: p. 1].

This thesis uses ACQUIRE version 1 dated May 1995. It is assumed that the MRTD points are already known, either from laboratory measurements or by running FLIR92, and therefore are treated as known model inputs.

C. DYNAMIC MODEL

For either spot detection or target discrimination, selecting a proper target size is crucial in obtaining consistent and accurate performance predictions. This "target size" is referred to as the target's *characteristic dimension,* based on the target's area. ACQUIRE has several weaknesses in this area. It depends upon: (1) a look up table that consists of only a limited set of military land vehicles, (2) having the user input only the target's height and length, or, (3) making off-line calculations in order to input the target's characteristic

dimension. These off-line calculations require that the user make a "best guess" at the predicted range of acquisition and then calculate the characteristic dimension for that range. This often results in the model having to be run multiple times in order to accurately predict the FLIR performance. If a target is not in the look up table, this becomes a very time consuming and cumbersome process. Another limitation in the ACQUIRE model is that the FORTRAN code uses only the target's length and height for the target's characteristic dimension calculations, and once calculated, this value does not change. This serves to give only a two dimensional view of the target and does not account for the changing target area associated with changes in range and azimuth. When calculating such things as projected target area, a three dimensional representation of a target will be much more accurate in predicting FLIR system performance, especially when using an airborne FLIR sensor. This model incorporates a three dimensional view of a target for the characteristic dimension calculations. This accounts for changes in the target's area based on range, the azimuth angle to the target, and the altitude of the FLIR sensor. The PASCAL code for the model can be found in Appendix A. For each increment of range we make the following calculations:

1. Total Atmospheric Transmittance

No matter how strong the target signature, the thermal signal is always attenuated to some degree by the intervening atmosphere. Attenuation occurs in the atmosphere by absorption and scattering of radiation. The most significant absorbers in the atmosphere are water, carbon dioxide, and ozone. The most important sources of scattering are water droplets suspended in air(rain or snow), dust, smoke, and smog [Ref. 5: p. 3.1]. The ratio of the intensity of usable radiation passing through a body of air and entering an optical system to the intensity originating from the source is known as *atmospheric transmittance* [Ref. 5: p. 3.1].

Several models exist for estimating infrared transmittance. The most widely accepted standard model is a computer program called LOWTRAN which evolved during the 1970's at the Air Force Geophysics Laboratory in Cambridge, Massachusetts [Ref. 5: p. 3.2]. For this thesis, none of the atmosphere models such as LOWTRAN were available, so the Dynamic Model calculates the *total atmospheric transmittance* of infrared radiation through the atmosphere as simply the product of the spectral transmittances due to absorption and aerosol scattering, and is given by:

$$T_A(\lambda) = T_a(\lambda)T_s(\lambda) \tag{3.1}$$

where

$T_A(\lambda)$ is the total spectral atmospheric transmittance at wavelength λ,

$T_a(\lambda)$ is the spectral transmittance due to absorption at wavelength λ,

$T_s(\lambda)$ is the spectral transmittance due to aerosol scattering at wavelength λ.

$T_A(\lambda)$ is a number between 0.0 and 1.0, where 1.0 means there is no loss in the atmosphere, and 0.0 is a total loss in the atmosphere.

The absorption coefficient, α, from Equation 2.5 is unknown, so the spectral transmittance due to absorption, $T_a(\lambda)$, is calculated based on humidity, the amount of water particles in the optical path, and the range [Ref. 5: p. 3.69]. The amount of water particles in the optical path is given by:

$$W_P = HR \tag{3.2}$$

where

H is the absolute humidity in precipitable centimeters per kilometer (pr cm/km)

$= 1.4e^{-1.357x10^{-4}Alt_m}$,

R is the range in kilometers.

Equation 3.2 is then used to calculate the spectral transmittance due to absorption and is determined by:

$$T_a(\lambda)=\frac{1}{1.06+0.19W_P+7.96x10^{-4}W_P^2+3.6x10^{-5}W_P^3+1.89x10^{-6}W_P^4} \quad (3.3)$$

The spectral transmittance due to aerosol scattering, $T_S(\lambda)$, is based on Equation 2.5 and is given by:

$$T_S=e^{-\alpha_S R} \quad (3.4)$$

where

α_s is the attenuation coefficient for aerosol scattering,

R is the range in kilometers.

In 1924, Koschmieder derived expressions for visual contrast of objects in the atmosphere that are useful for estimating meteorological visibility conditions of the ambient atmosphere. This Koschmieder relation is used extensively in propagation models to establish a volume attenuation coefficient at visible wavelengths when a meteorological visibility or visual range is known [Ref. 10: Vol 7 p. 476]. Table 3.1 shows the attenuation coefficients for aerosol scattering, α_s, for different IR wavelength bands using the Koschmieder relation.

Wavelength	Attenuation coefficient (α_s)
0.4 - 0.7 μm	3.91/Visual Range
0.7 - 1.1μm	2.35/Visual Range
3 - 5 μm	2.24/Visual Range
8 - 12 μm	0.85/Visual Range

Table 3.1: Koschmieder Relationship for Determining α_S.

All values for the total atmospheric transmittance at each range, calculated in the Dynamic Model, were used as the transmittance inputs for the ACQUIRE version 1 model.

2. Apparent Target-To-Background Temperature Differential

The apparent target-to-background temperature differential at the sensor is found by multiplying the actual target-to-background temperature differential, ΔT measured in degrees Celsius, by the total atmospheric transmittance. This is:

$$\Delta T' = \Delta T T_A. \tag{3.5}$$

3. Characteristic Dimension

The area of the target that is of concern for proper FLIR analysis is the projected area normal to the line-of-sight from the sensor to the target. This area is dependent on the target dimensions, the observing aspect, and whether or not the target is obscured by the horizon [Ref. 5: p. 2.10]. The distance to the horizon in kilometers is calculated by $3.57\sqrt{Alt_m}$ or nautical miles by $1.23\sqrt{Alt_{Feet}}$. The amount of the target's height obscured by the horizon is given by [Ref. 5: p. 2.16]:

$$h_o = \frac{R^2}{2r_e} - R\sqrt{\frac{2Alt_m}{r_e}} + Alt_m \tag{3.6}$$

where

R is the range in meters from sensor to target (R > distance to horizon),

Alt_m is sensor altitude in meters,

r_e is the radius of the earth = 6.37×10^6 meters.

This obscured height is then subtracted from the height of the target yielding an observable height of target, h:

$$h = \text{Height of Target} - h_o. \tag{3.7}$$

The target aspect is expressed in terms of elevation angle, θ, and azimuth angle, ϕ. For example, for the beam of a ship viewed from sea level, the elevation angle is 0° and the azimuth is 90° [Ref. 5: p. 2.15]. The area of a target is given by:[2]

$$A_T = lw\sin\theta + hw\cos\theta\sqrt{(1-\sin^2\phi\cos^2\theta)} + hl\cos\theta\sqrt{(1-\cos^2\phi\cos^2\theta)} \tag{3.8}$$

where

- h is the unobscured target height, found in Equations 3.6 - 3.7,
- w is the target width,
- l is the target length,
- ϕ is the azimuth angle,
- θ is the elevation angle.

The derivation of Equation 3.8 is found in Appendix B. The target's characteristic dimension is then the square root of the target's area, or given by:

$$D_C = \sqrt{A_T} \tag{3.9}$$

---

[2] There is an equation (2.1) on page 2.15 of Ref 5 that claims to give A_T for any θ and ϕ. Using this formula, if the target is approached from the front ($\phi = 0°$), as θ approaches 90° (overhead view) one gets lw, the correct value for A_T. However, for any value of $\phi > 0°$ it gives an incorrect answer. In particular, if the target is approached from the side ($\phi = 90°$), as θ approaches 90° (overhead view) it gives $A_T = 0$. Equation (3.8) above gives the correct A_T for all values of θ and ϕ.

where

D_C is the target's characteristic dimension.

4. Resolvable Cycles

In order to compute the resolvable cycles across the target's characteristic dimension, the *spatial frequency* of the target, υ_R , must be computed. *Spatial frequency* is used to describe an object, its image, and the imaging characteristics of systems designed to view those images. This is done by finding the frequency where the MRTD is equal to $\Delta T'$ (Equation 3.5). Once the spatial frequency of the target is determined, then the number of resolvable cycles across the target's characteristic dimension is calculated by:

$$N_R = \frac{\upsilon_R D_C}{R} \tag{3.10}$$

where

υ_R is the spatial frequency of the target in cycles/mRad,

D_C is the target's characteristic dimension in meters, Equation 3.9,

R is the range to the target in meters.

5. P Infinity

The probability of acquiring a target given that it is in the sensor field of view and provided infinite search time is given by: [Ref. 12: p. 4]

$$P_{INF} = (N_R/N_{50})^F/(1 + (N_R/N_{50})^F) \tag{3.11}$$

where

F is a correction factor (Duvoisin, et al., 1984) = $2.7 + 0.7(N_R/N_{50})$,

N_R is resolvable cycles across target's characteristic dimension, Equation 3.10,

N_{50} is the number of cycles required across target from Johnson's criteria, found in Table 2.3.

The complete Dynamic Model is implemented in PASCAL code, and is contained in Appendix A.

IV. MODEL ANALYSIS

The focus of this thesis is to analyze the effects of dynamically calculating a target's characteristic dimension on the results from FLIR performance prediction models. In order to do this, several runs of ACQUIRE version 1 and the Dynamic Model were made against a theoretical target of dimension 100 meters x 20 meters x 10 meters for varied approach angles. Results from the models are then compared to actual data from an experiment conducted jointly by the Naval Postgraduate School and the Naval Command, Control and Ocean Surveillance Center, RDT&E Division (NRaD) off the coast of Monterey, CA.

Because FLIR MRTD's are proprietary in nature, and most contractors are reluctant to provide these numbers, the system used in the NRaD experiment and its associated parameters are used for all of the following characteristic dimension analysis. The FLIR system modeled is the AN/AAS-36 infrared detecting set (IRDS) manufactured by Texas Instruments. It operates in the 8 - 12 μm wavelength, and has a wide to narrow FOV ratio equal to 3°.

A. ACQUIRE vs. DYNAMIC AGAINST THEORETICAL TARGET

In this analysis all inputs to each model are the same with the exception of the varied angle of approach. The Dynamic Model uses approach angle as input from the user to calculate the characteristic dimension (Equations 3.8 and 3.9). The ACQUIRE model takes the characteristic dimension, directly, as input. Off-line calculations were performed to determine this input from the various angles. This was accomplished by taking the square root of the two dimensional area seen from the approach angle. For example, if the approach is from the front, then ACQUIRE calls for an input of $\sqrt{hw}$ as the characteristic dimension equation. A theoretical target with dimensions (l, w, h) 100 x 20 x 10 meters is

used, the FLIR sensor is at an altitude of 500 FT, the target has a temperature differential with its background, ΔT, of 4° Celsius, and visibility is taken to be 10 nautical miles.

1. Front View ($\phi = 0°$)

For the front view, ACQUIRE is run with a target characteristic dimension equal to $\sqrt{hw}$. This results in the calculation of $\sqrt{10x20} = 14.14$ meters. As can be seen in Figure 4.1, as range to target decreases, the characteristic dimension increases. The difference from ACQUIRE's static characteristic dimension results from the greater target area being recognized by the Dynamic Model. For this run, at 500 feet altitude, the Dynamic Model "sees" a characteristic dimension of 14.67 meters, or an increase of 4% at the 30 kilometer range. This increase in characteristic dimension steadily grows by 81% to 25.56 meters at a range of 1 kilometer.

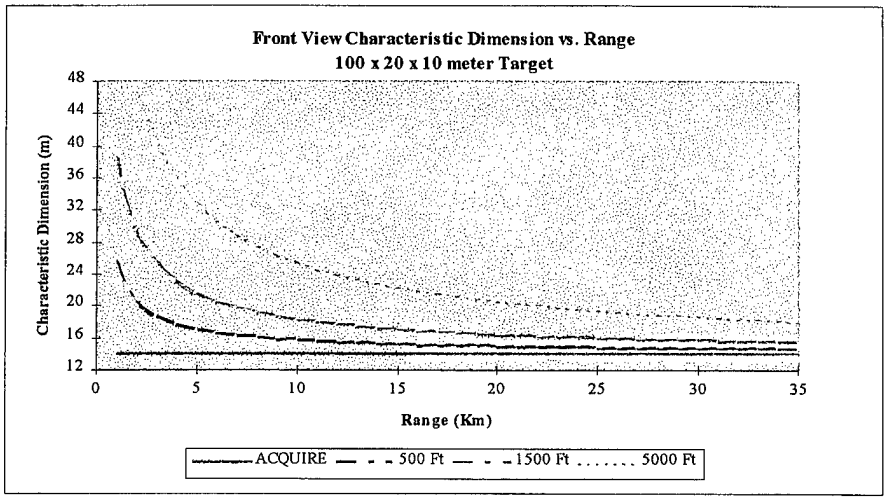

Figure 4.1: Front View Comparison of Characteristic Dimension for Given Altitudes.

Also of note is that when the altitude of the sensor is increased, the difference between ACQUIRE's characteristic dimension and the dynamically calculated characteristic dimension becomes even more significant. This results in greater prediction ranges for the

Dynamic Model.

Columns 2 and 3 of Table 4.1 depict the predicted range where detection will occur for ACQUIRE and the Dynamic Model, respectfully, for each of the associated probabilities in column 1. Column 4 shows the % difference between the models. For the front view of the 100 x 20 x 10 meter target, the dynamic model yields an average of 8% greater prediction ranges over the ACQUIRE model. This is attributed to the use of a larger characteristic dimension for any given range, calculated in the Dynamic Model.

Probability	ACQUIRE	DYNAMIC	Δ %
0.95	9.33	10.22	10
0.90	10.53	11.41	8
0.85	11.29	12.28	9
0.80	11.94	13.02	9
0.75	12.53	13.64	9
0.70	13.09	14.25	9
0.65	13.65	14.84	9
0.60	14.21	15.40	8
0.55	14.79	15.99	8
0.50	15.41	16.57	8
0.45	16.07	17.19	7
0.40	16.79	17.84	6
0.35	17.42	18.52	6
0.30	18.10	19.26	6
0.25	18.90	20.10	6
0.20	19.91	21.10	6
0.15	21.00	22.28	6
0.10	22.39	23.83	6
0.05	24.85	26.27	6

Table 4.1: Model Output for Front View.

2. 45° View ($\phi = 45°$)

For the 45° view, ACQUIRE is run with a target characteristic dimension equal to $\sqrt{(hlsin45)+(hwcos45)}$. This results in the calculation of $\sqrt{(10x100sin45)+(10x20cos45)}$ = 29.13 meters. Figure 4.2 shows that from this angle, at 10 kilometers and 500 feet elevation, the target's characteristic dimension is dynamically calculated, using equations 3.8 and 3.9, to be 29.65 meters, or 2% greater. As the range to target decreases, this difference increases to 17%, corresponding to a characteristic dimension of 33.96 meters. The effect of altitude is similar to that seen in Figure 4.1.

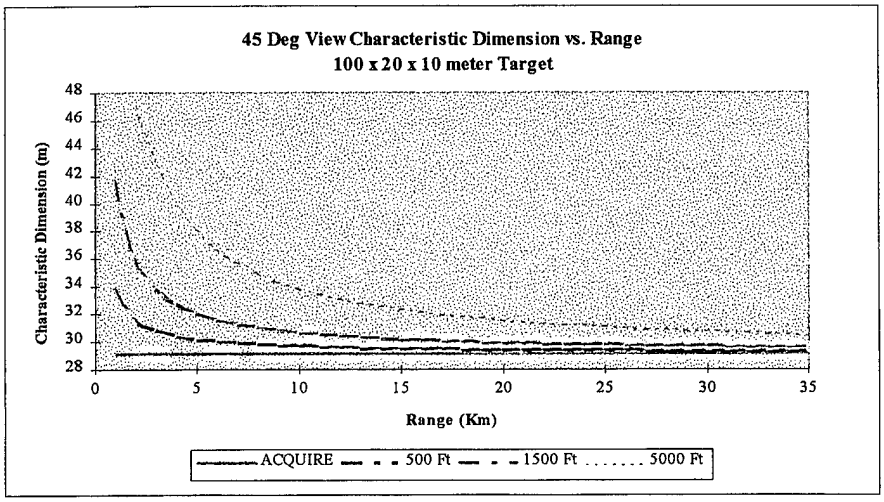

Figure 4.2: 45° View Comparison of Characteristic Dimension for Given Altitudes.

Table 4.2 depicts the output for the 45° view of the 100 x 20 x 10 meter target, with the Dynamic Model yielding an average of 4% greater prediction ranges over the ACQUIRE model.

Probability	ACQUIRE	DYNAMIC	Δ %
0.95	15.51	16.10	4
0.90	17.18	17.72	3
0.85	18.15	18.81	4
0.80	18.96	19.67	4
0.75	19.71	20.42	4
0.70	20.41	21.12	3
0.65	20.90	21.74	4
0.60	21.39	22.32	4
0.55	21.89	22.90	5
0.50	22.39	23.45	5
0.45	22.93	24.03	5
0.40	23.51	24.61	5
0.35	24.15	25.23	4
0.30	24.78	25.89	4
0.25	25.31	26.55	5
0.20	25.93	27.29	5
0.15	26.72	28.16	5
0.10	27.81	29.26	5
0.05	29.20	30.87	6

Table 4.2: Model Output for 45° View.

3. Side View ($\phi = 90°$)

For the side view, ACQUIRE is run with a target characteristic dimension equal to $\sqrt{lh}$. This results in the calculation of $\sqrt{100x10} = 31.6$ meters. In Figure 4.3 you can see that again at a range of 10 kilometers and 500 feet elevation, the dynamic characteristic dimension is 32.10 meters or 2% greater than that of ACQUIRE. This difference increases to 15% at 1 kilometer, corresponding to a characteristic dimension of 36.38 meters. Changes in altitude again have the same effects as in Figures 4.1 and 4.2.

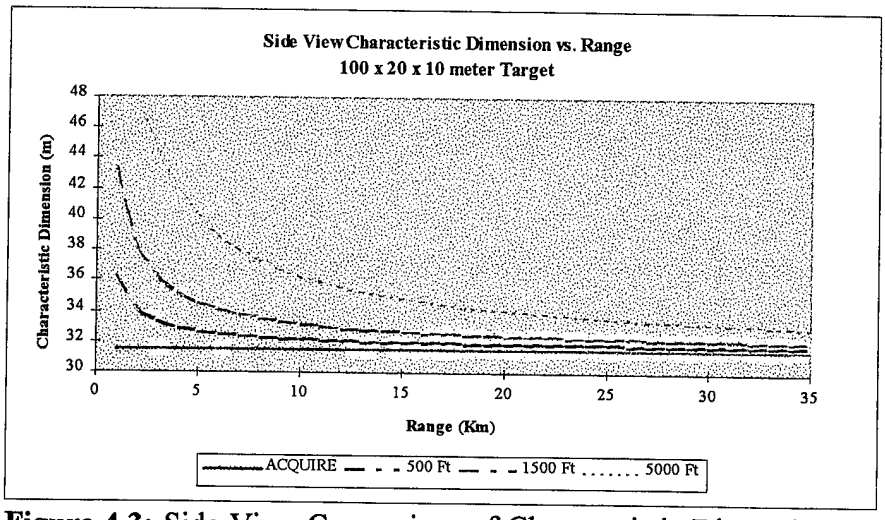

Figure 4.3: Side View Comparison of Characteristic Dimension for Given Altitudes.

Table 4.3 depicts the output for the side view of the 100 x 20 x 10 meter target, with the Dynamic Model yielding an average of 5% greater prediction ranges over the ACQUIRE model.

The most notable differences between the outputs of the Dynamic Model and ACQUIRE are seen when in close proximity to the target or when approaching the target from the front/back. This is where the effects of the dynamically calculated characteristic dimension are most obvious over the static characteristic dimension. The effects of using a three dimensional view of a target instead of the two dimensional view yields a greater target area, and hence, a greater target characteristic dimension. This results in the greater prediction ranges seen in Tables 4.1 - 4.3. As range from target increases, these effects are not as pronounced, and therefore there is less difference between the ACQUIRE model's calculations and the Dynamic Model. But if altitude is increased, as shown in Figures 4.1-4.3, then the Dynamic Model becomes significantly different from ACQUIRE. This difference is important when evaluating airborne FLIR systems against surface targets.

Probability	ACQUIRE	DYNAMIC	Δ %
0.95	16.43	16.97	3
0.90	17.94	18.56	3
0.85	18.95	19.65	4
0.80	19.82	20.52	4
0.75	20.54	21.28	4
0.70	21.07	21.97	4
0.65	21.59	22.54	4
0.60	22.09	23.12	5
0.55	22.61	23.67	5
0.50	23.14	24.23	5
0.45	23.70	24.79	5
0.40	24.30	25.36	4
0.35	24.83	25.98	5
0.30	25.31	26.55	5
0.25	25.85	27.19	5
0.20	26.47	27.90	5
0.15	27.28	28.72	5
0.10	28.30	29.77	5
0.05	29.58	31.29	6

Table 4.3: Model Output for Side View.

B. EXPERIMENTAL DATA

Since the dynamically calculated characteristic dimension provides a greater theoretical probability of detection at any given range, the analysis shifts to see how predictions produced by the two models compare to the results found in an actual FLIR acquisition scenario. The data for this part of the analysis were published in a Naval Postgraduate School Masters Thesis by Jon C. Kreitz, December, 1992 [Ref. 7], and are included in Table 4.4. They were collected in conjunction with an experiment conducted

off the coast of California in order to evaluate the PREOS program for determining acquisition ranges of airborne FLIR systems. On August 4, 1992, a P-3 Maritime Patrol Aircraft equipped with the AN/AAS-36 Infrared Detecting Set (IRDS) conducted 8 overflights of the Research Vessel *PT SUR* from various altitudes and target angles. The dependent variables for the experiment were range of detection, classification, and identification. For this thesis, only the detection range is used for analysis purposes, although the results can be applied to the other visual discrimination tasks as well. Detection range is defined as the point when the Sensor 3 operator (the P-3 air crewman) detected a dot on his FLIR video display screen and is measured in Kilometers (Km). Table 4.4 contains the data set from the experiment.

Run	Time (Zulu)	Altitude (Feet)	Target Angle (ϕ)	FLIR Detection Range (Km)
1	0411	1027	270	21.1
2	0425	1008	070	14.7
3	0432	1020	180	12.8
4	0441	1013	000	14.7
5	0449	457	090	22.0
6	0503	508	270	15.6
7	0511	538	090	22.0
8	0522	530	270	15.6

Table 4.4: Experimental Data Set.

The R/V *PT SUR* has dimensions (l,w,h) of 41.2 x 9.76 x 15.24 meters. The conditions at the time of the experiment were clear skies, 14 NM visibility, and a ΔT of 4°C. The P-3 recorded 4 overflights at 500 feet, and 4 overflights at 1000 feet. With only eight data points available, an altitude of 750 feet was used in the model, rather than split the data into two distinct sets of four observations at different altitudes.

1. Empirical Distribution

The data in Table 4.4 can be broken into two groups, the two runs with bow/stern (0°/180°) target angles and the six runs with beam (90°/270°) target angles. Using Equations 3.8 and 3.9, the characteristic dimension for each detection was then calculated and graphed vs. its actual detection range, shown in Figure 4.4. Because you get the same characteristic dimension for the 0° and 180° runs, and the same characteristic dimension for the 90° and 270° runs, the data were grouped into two categories, those with a characteristic dimension approximately 12 meters and those with a characteristic dimension of approximately 25 meters.

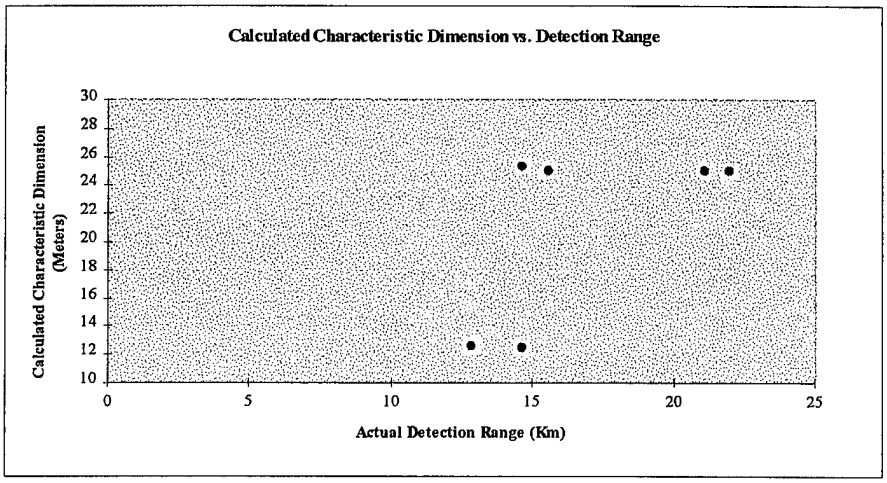

Figure 4.4: Calculated Characteristic Dimension vs. Actual Detection Ranges for *PT SUR* Experimental Data.

With the data broken into the two groups, an empirical Cumulative Tail Distribution for each characteristic dimension was then calculated. This was determined by dividing the number of detections that occurred at distances greater than a given range, *r*, by the total number of observations for each characteristic dimension. Figure 4.5 shows the distribution for a characteristic dimension of 25 meters. The reader can see that 95% probability of detection occurs at approximately 15.5 km, and 5% probability of detection occurs at

approximately 23.5 km. Despite only two data points for the characteristic dimension of 12 meters, the Cumulative Tail Distribution was calculated because the Dynamic Model demonstrated the greatest variation from the ACQUIRE model against the theoretical target from the front view of a target, as discussed in Section A above. Figure 4.6 shows the empirical distribution with a 95% probability of detection occurring at approximately 13.2 km and the 5% probability occurring at approximately 15.8 km.

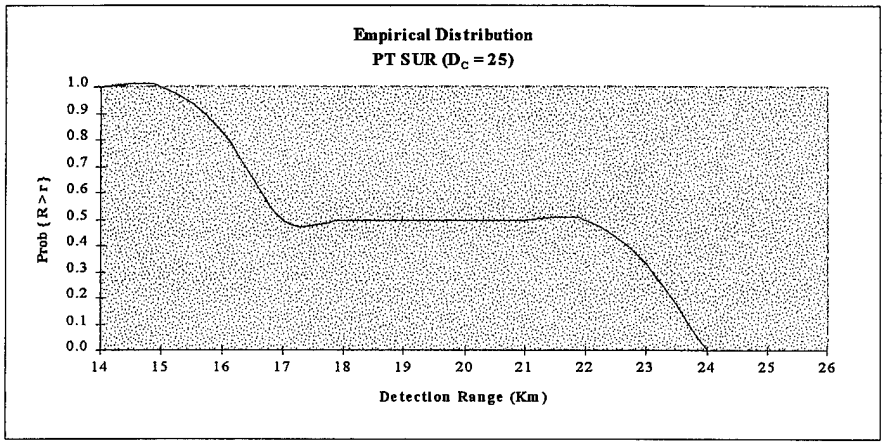

Figure 4.5: Cumulative Tail Distribution for R/V *PT SUR* with a Characteristic Dimension of 25 Meters.

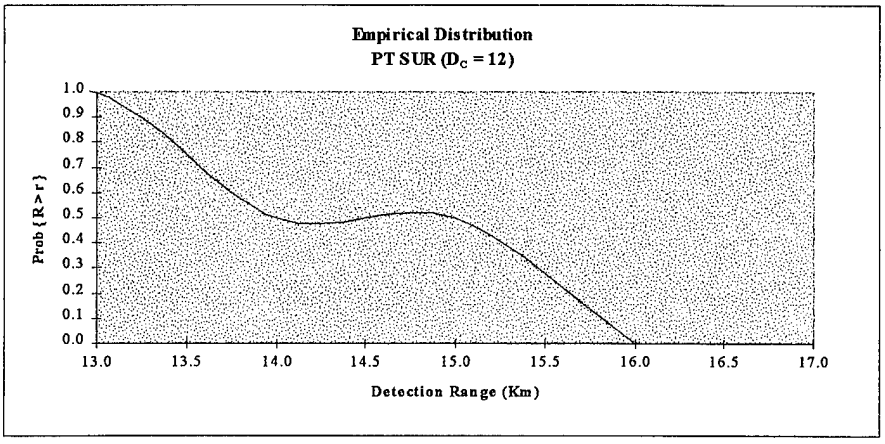

Figure 4.6: Cumulative Tail Distribution for R/V *PT SUR* with a Characteristic Dimension of 12 Meters.

2. Model Inputs

The major input to both models is a file that contains the MRTD and corresponding spatial frequency data points associated with the particular FLIR system being tested. Because these numbers are proprietary in nature, they are not be published here. For this thesis the file contained 20 such points for Texas Instruments' AN/AAS-36, and the same file was used by both models. Table 4.5 summarizes the rest of the inputs for both models taken from the conditions that existed at the time of the experiment.

INPUT	ACQUIRE	DYNAMIC
Field of View (FOV)	Wide	Wide
Wide-Narrow FOV Ratio	3.0°	3.0°
Target Data	D_c = 12.19 D_c = 25.06	Length = 41.2 m (135 ft) Width = 9.76 m (32 ft) Height = 15.24 m (50 ft)
Azimuth (Target Angle)	Not Required	0° or 90°
Δ T	4.0° C	4.0° C
Johnson Cycle Criteria	Detection_n50 = 0.75	Detection_n50 = 0.75
Transmittance	Input from calculations from Dynamic Model	Not Required
Visibility	Not Required	14 NM
Altitude	Not Required	750 ft
I/R Band of Interest	8 - 12 μm	8 - 12 μm

Table 4.5: Summary of Inputs for Model Comparison.

3. Model Output vs. Empirical Distribution

Each model produces a theoretical Probability of Detection vs. Range (Km), which then can be graphed to produce an acquisition probability curve. Table 4.6 summarizes the results, and these are graphically displayed in Figure 4.7 and Figure 4.8. For the 12 meter characteristic dimension (ϕ = 0°), the Dynamic Model predicts a detection range on the average of 4% greater than the ACQUIRE model. For the 25 meter characteristic

dimension ($\phi = 90^{o}$), the detection range prediction is an average of 1% greater. These differences can be explained by the fact that the ACQUIRE model's characteristic dimension is fixed at either 12.19 or 25.06 meters, and the Dynamic Model's characteristic dimension, although continuously changing, never gets below these values because of the inclusion of the target's third dimension into the calculations. That means the target area that is seen by

	Characteristic Dimension (D_c) = 12 Meters			Characteristic Dimension (D_c) = 25 Meters		
Prob	**ACQUIRE**	**DYNAMIC**	**Δ %**	**ACQUIRE**	**DYNAMIC**	**Δ %**
0.95	8.54	9.13	7	14.79	15.07	2
0.90	9.67	10.27	6	16.42	16.74	2
0.85	10.52	11.14	6	17.65	17.95	2
0.80	11.25	11.86	5	18.70	18.94	1
0.75	11.93	12.49	5	19.68	19.80	1
0.70	12.54	13.11	5	20.52	20.57	0
0.65	13.06	13.68	5	21.19	21.30	1
0.60	13.59	14.26	5	21.86	22.01	1
0.55	14.14	14.85	5	22.55	22.69	1
0.50	14.71	15.45	5	23.26	23.39	1
0.45	15.32	16.09	5	24.02	24.11	0
0.40	15.99	16.77	5	24.76	24.82	0
0.35	16.74	17.51	5	25.42	25.56	1
0.30	17.61	18.35	4	26.15	26.36	1
0.25	18.65	19.31	4	27.00	27.25	1
0.20	19.97	20.46	2	28.06	28.27	1
0.15	21.34	21.85	2	29.45	29.48	0
0.10	23.29	23.77	2	30.77	30.94	1
0.05	26.28	26.78	2	32.94	33.10	0

Table 4.6: Model Output of Theoretical Detection Range in Kilometers.

the sensor is always greater than the ACQUIRE model, therefore the probability of detection for a given range is always greater, leading to the greater prediction ranges. In Figures 4.7 and 4.8 you can see how the results from each model compare to the empirical distribution from the experimental data.

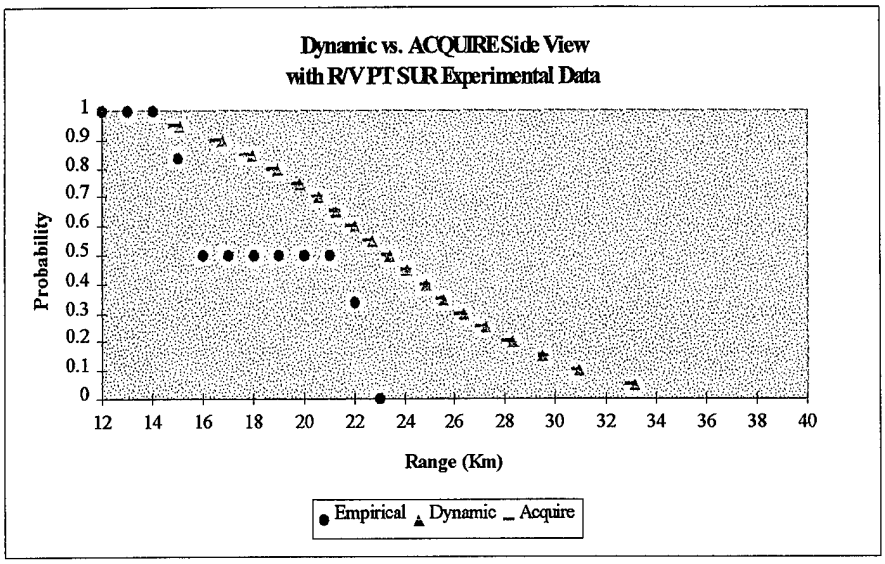

Figure 4.7: Model Output Compared to Empirical Distribution for Side View of R/V *PT SUR*.

The reader will notice in Figure 4.7, that for the side view of the R/V *PT SUR*, both models accurately predict the detection ranges for the 90% to 100% probability range, with the Dynamic Model having the 1% greater prediction ranges as previously mentioned. However, the empirical distribution does not reflect the general shape of the curve below these points. This may be a result of only having six data points to predict the distribution shape.

In Figure 4.8, the front view of the R/V *PT SUR*, both models under predict the performance of the FLIR in the 75% to 100% probability ranges, with the Dynamic Model having the 4% greater prediction ranges mentioned above. Recall that there are only two

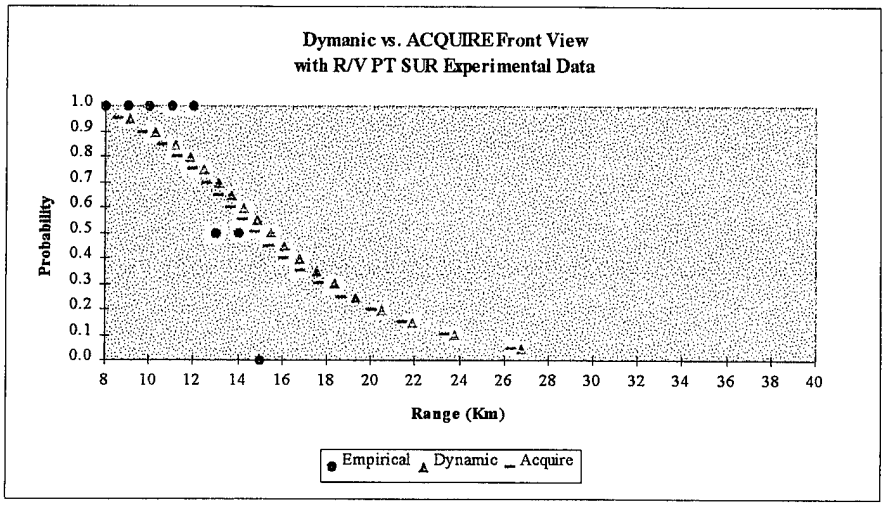

Figure 4.8: Model Output Compared to Empirical Distribution for Front View of R/V *PT SUR*.

actual observations that make up this distribution. The point that is being stressed here is the fact that both models under predict the top 25% of detection ranges. So from a modeling standpoint, the Dynamic Model, with its 4% greater prediction ranges, is closer to predicting the actual detection ranges of the AN/AAS-36 on the Research Vessel *PT SUR*.

There could be several reasons to explain differences between actual and predicted ranges of FLIR performance. For example:

- Accuracy of the Δ T measurement throughout the experiment.
- Accuracy of the measurement of the atmospheric conditions such as temperatures, pressures, humidity, and visibility.
- Experimental test bias - The operator (air crewman) declares when he/she makes a detection, recognition, or identification. This is highly subjective and extremely variable from person-to-person.
- The Empirical Distribution was compiled from a limited data set. An increased number of data points will lead to a better representation of the actual distribution.

Any one of these factors or a combination of all could explain any variation between the predicted and the actual detection ranges.

The next section demonstrates how changes to model parameters affect the prediction ranges obtained from the models. Since both models are similar with the exception of the characteristic dimension calculations, the focus of the sensitivity analysis is on the Dynamic Model, although the same effects could be demonstrated using the ACQUIRE model.

C. DYNAMIC MODEL SENSITIVITY ANALYSIS

The sensitivity of the FLIR prediction models to various inputs may explain any disparity seen between theoretical predictions and empirical detection ranges. Since there is no way to account for operator bias in theoretical predictions without further human factors experimentation, this will not be addressed any further. However, examining the effects of ΔT, visibility/transmissivity, and altitude may account for differences between FLIR prediction models and actual observed detection ranges. For the following sensitivity analysis, the inputs into the Dynamic Model were from the R/V *PT SUR* acquisition scenario. We define those inputs as the "Base Case." The azimuth, or attack angle, used in all runs is the front view ($\phi = 0°$). This view was chosen because it yielded the largest difference between the ACQUIRE model and the Dynamic Model in both the hypothetical and R/V *PT SUR* analysis.

1. ΔT

Accurate measurement of ΔT is always difficult, but recent advances in technology now allow for reliable measure of scene temperatures. If ΔT is estimated in data collection, the result could cause significant differences between actual detection ranges and predictions. The base case for ΔT was set at 4° C, and was varied from 2° C to 6° C. Figure 4.9 displays the results of varying ΔT. For each 0.5° C increase in target to background temperature differential, the Dynamic Model yielded a 2% increase in predicted

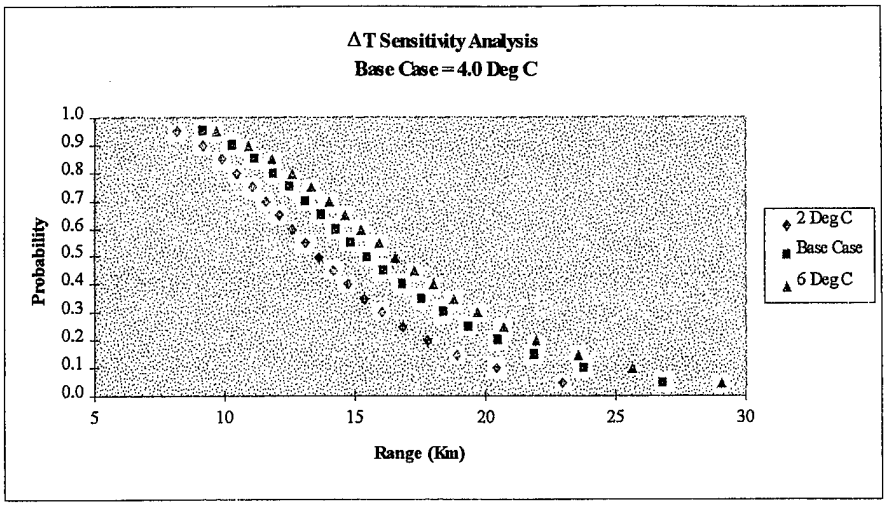

Figure 4.9: Model Sensitivity to Target to Background Temperature Differential.

detection range. As ΔT approaches 0° C, meaning it's harder to discriminate a target from its background, every 0.5° C decrease yields a 3% decrease in predicted detection range.

2. Visibility

For the Dynamic Model, transmittance is calculated from a procedure based on humidity, range, and visibility, Equations 3.1 - 3.4. Of the three, visibility is the only variable because humidity is a function of the sensor's altitude, and the Dynamic Model accounts for range in increments of 1 kilometer. So in order to analyze the effects of transmittance on prediction ranges, visibility is varied in 5 NM increments, where the Base Case is 14 NM. Figure 4.10 shows that in cases with low visibility, approximately 5 NM, there is a 13% increase in predicted detection range for a 5 NM increase in visibility. Having greater that 10 NM visibility yields a 3% increase in predicted detection ranges for each 5 NM increment.

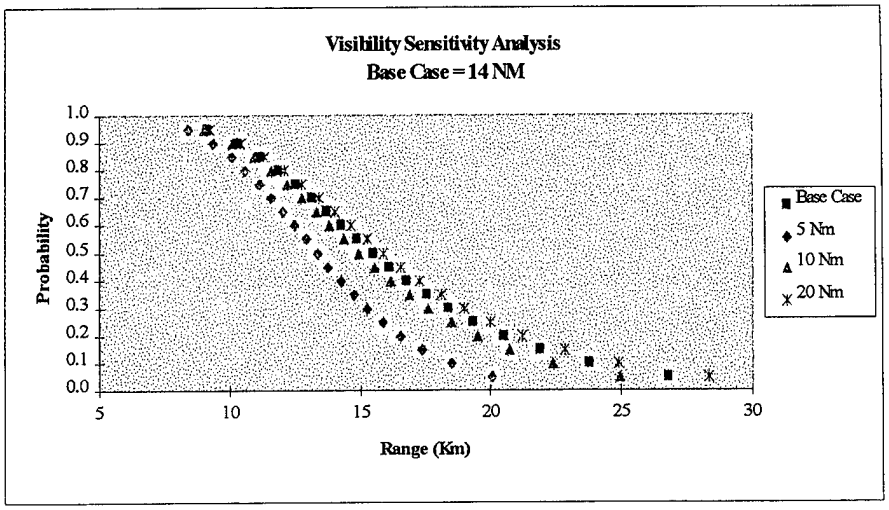

Figure 4.10: Model Sensitivity to Visibility/Transmittance.

3. Altitude

As shown in Figures 4.1 - 4.3, altitude has a significant effect on the characteristic dimension. At low altitudes, the characteristic dimension is not going to vary that much. As altitude increases, the characteristic dimension increases, because the area of the target is increasing. With a greater target area, the probability of detection must increase for all ranges. Figure 4.11 shows these results. Each increment of altitude increased the predicted detection ranges by 5%.

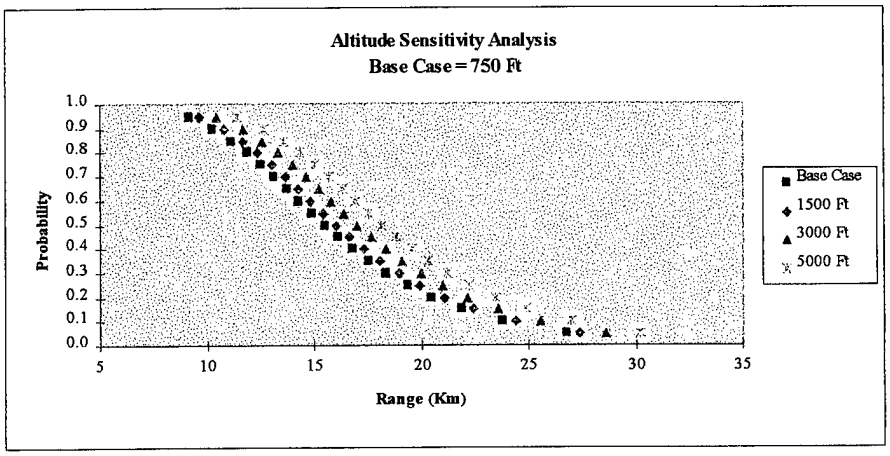

Figure 4.11: Model Sensitivity to Altitude.

V. CONCLUSIONS

A. SUMMARY

This thesis presents an analysis of the effects on model output of dynamically calculating a target's characteristic dimension used in FLIR performance prediction models. The models used are ACQUIRE version 1 and the Dynamic Model, which make identical calculations except in the area of the target's characteristic dimension. Both models are compared on a theoretical target from three different angles, the front (ϕ=0°), the 45 (ϕ=45°), and the side (ϕ=90°). The Dynamic Model produces an 8% increase in prediction ranges for the front view, a 4% increase for the 45° view, and a 5% increase for the side view. An Empirical Cumulative Tail Distribution is computed from experimental data. Despite the small sample size from the experiment, both models' predictions compare favorably against the actual detection ranges. For the front view, the Dynamic Model provided 4% longer prediction ranges, a closer representation of the empirical distribution. A sensitivity analysis is then performed on the Dynamic Model to demonstrate how various model inputs affect the predicted detection ranges.

B. COMMENTS

From the onset of this project, it has been clear that FLIR industry analysts recognize the shortcomings in testing FLIR systems. The reason to have a model is to provide some insight of the overall performance of the system. It is unlikely that the output of a model would match field test data in an absolute comparison of system capability. However, the goal is to be as accurate as possible. This thesis demonstrates that the Dynamic Model's characteristic dimension calculations yield greater prediction ranges over ACQUIRE, particularly when viewing a target from the front.

The limited data set discussed in Chapter IV, and the sometimes incomplete information about environmental conditions, points out the need to conduct field testing on a calibrated range, with precise recording of the environmental conditions. Only then can a comparison be made to determine how good the predictions from the Dynamic Model are.

APPENDIX A. PASCAL IMPLEMENTATION CODE

A. DISCLAIMER

The reader is cautioned that the computer program developed in this research may not have been exercised for all cases of interest. While every effort has been made, within the time available, to ensure that the program is free of computational and logic errors, it cannot be considered validated. Any application of this program without additional verification is at the risk of the user.

B. PASCAL CODE

```
program flir;

{$N+}

{
  Author: Lt. J. P. Eaton
  Date:   March 1997
  Description: This program takes as inputs: Target Dimensions; Atmospheric conditions; MRT data and
  FLIR parameters to produce a dynamic model of FLIR performance. It takes the range to target, and
  dynamically re-calculetes the target's chareacteristic dimension based on closure to target. The model
  assumes azimuth angle will remain constant - off the nose - to simulate an intercept. The MRT points are
  read from a data file and the program prints the results in Flir.out and the Probability Array in Flir.prb.
}

uses wincrt;

const
  MaxArraySize = 250;
  EarthRad = 6370000;   { radius of earth in meters = 6.37 x 10^6 }

type
  MrtData = record
            Freq : real;
            Mrt  : real;
          end;
  ProbData = record
```

```
        Rng  : real;
        Prob : real;
      end;

var
  Infile, Probfile : text;
  ArraySize, RngInc : integer;
  DataArray : array[1..MaxArraySize] of MrtData;
  ProbArray : array[0..MaxArraySize] of ProbData;
  Length, Height, Width, Azimuth, Vis : real;
  Range, Alt, AltM, Trnsmiss, DeltaT, DeltaTPrime : real;
  Cycles, Wide2Narrow, VsubR, CritDem, Prob : real;
  RunFlag, IRband, JohnCrit, FOV : char;

{ ********************************************************** }

function NmToKm (num : real) : real;  { 1NM = 0.5393KM }

  begin
    NmToKm := num/0.5393;
  end;

{ ********************************************************** }

function KmToNm (num : real) : real;

  begin
    KmToNm := num * 0.5393;
  end;

{ ********************************************************** }

function power (num : real; expnt : real) : double;

  begin
    if expnt = 0.0 then
      begin
        power := 1.0;
      end
    else
      begin
        if num = 0.0 then
          begin
            power := 0.0;
          end
        else
          begin
            power := Exp(expnt * (ln(num)));
          end;
```

```
      end;
  end;

{  ********************************************************  }

function log10 (num : real) : real;

  begin
    if num > 0.0 then
      begin
        log10 := ln(num)/ln(10);
      end
    else
      begin
        log10 := 0.0;
        writeln('ERROR - Ln of zero: log10');
      end;
  end;

{  ********************************************************  }

function LogInterp (y2, y1, ydt, x2, x1 : real) : real;

  var                          { Interpolates between 2 numbers }
    slope, intrcpt : extended;

  begin
    if (y2 = 0.0) or (y1 = 0.0) then LogInterp := 0.0;
    if x2 = x1 then
      begin
        slope := 0.0;
        writeln ('ERROR LogInterp : Division by zero!');
      end
    else
      begin
        slope := (log10(y2/y1))/(x2-x1);
      end;
    if slope = 0.0 then
      begin
        LogInterp := 0.0;
      end
    else
      begin
        intrcpt := log10(y2) - slope * x2;
        if (log10(ydt) - intrcpt)/slope > 0.0 then
          begin
            LogInterp := (log10(ydt) - intrcpt)/slope;
          end
        else
```

```
        LogInterp := 0.0;
      end;
  end;

{  ********************************************************  }

function ArcSin (Opp, Hypot : extended) : extended;

  var
    Adj, X : extended;    { Developed because PASCAL only uses TAN function}

  begin
    Hypot := Hypot * 1000;
    if Hypot < Opp then
      begin
        Adj := 0.0;
      end
    else
      begin
        Adj := Sqrt(Sqr(Hypot) - Sqr(Opp));
      end;
    if Opp = 0.0 then
      begin
        ArcSin := 0.0;
      end
    else
      begin
        X := ArcTan(Adj/Opp) * (180/Pi);    { convert rads to degs }
        ArcSin := 90 - X;
      end;
  end;

{  ********************************************************  }

procedure Initialize;

  var
    index : integer;

  begin
    for index := 1 to MaxArraySize do
      begin
        DataArray[index].Freq := 0.0;
        DataArray[index].Mrt := 0.0;
        ProbArray[index - 1].Rng := 0.0;
        ProbArray[index - 1].Prob := 1.0;
      end;
    ArraySize := 0; RngInc := 1;
    Length := 0.0; Height := 0.0; Width := 0.0; Azimuth := 0.0;
```

```
    Vis := 0.0; Range := 0.0; Alt := 0.0; AltM := 0.0; Trnsmiss := 0.0;
    DeltaT := 0.0; DeltaTPrime := 0.0; Cycles := 0.0; VsubR := 0.0;
    CritDem := 0.0; Prob := 0.0; Wide2Narrow := 0.0;
  end;

{  ********************************************************  }

procedure GetData;

var
  index : integer;
  freq, mrt : real;

begin
  writeln('MRT Data:');
  writeln('How many MRT data points do you want to enter?');
  readln (Infile,ArraySize);
  writeln; writeln;
  writeln('Now enter the MRT data:');
  writeln; writeln('Enter the data in the form of: ');
  writeln(' Freq<space>MRT<crt) ');
  for index := 1 to ArraySize do
    begin
      read(Infile,freq,mrt);
      DataArray[index].Freq := freq;
      DataArray[index].Mrt := mrt;
    end;
  writeln('The ',index,' data points entered are as follows: ');   writeln;
  for index := 1 to ArraySize do
    begin
      writeln(DataArray[index].Freq :8:4,' , ',DataArray[index].Mrt :8:4);
    end;
  writeln;writeln('Press any Key to continue:');
  RunFlag := readkey;
  writeln; writeln; writeln('Target Data:');
  writeln('Please enter the targets LENGTH, WIDTH, and HEIGHT in METERS: ');
  readln (Length, Width, Height);    writeln;
  repeat
    writeln('Enter Azimuth Angle to target:');
    writeln('0 Deg for head-on or bow - 90 Deg for beam approach.');
    readln(Azimuth);
  until (Azimuth >= 0.0) and (Azimuth <= 90.0);
  writeln; writeln;
  Range := 30;
  Range := NmToKm(Range);
  writeln; writeln; writeln('Enviormental Data:');
  writeln('Now enter altitude in feet');
  readln(Alt);
  AltM := Alt/3.28;                    { convert Alt to meters }
```

```
  writeln('Enter visibility in NM - IF UNLIM, ENTER 25 NM');
  readln(Vis);
  Vis := NmToKm(Vis);
  writeln('Enter Temperature Differential between target and backround; Delta T');
  readln(DeltaT);
  writeln; writeln; writeln('FLIR Data:');
  writeln; writeln('Enter IR band of interest:');
  writeln('          A. Visible : 0.4 - 0.7 um');
  writeln('          B. Near    : 0.7 - 1.1 um');
  writeln('          C. Thermal : 3.0 - 5.0 um');
  writeln('          D. Thermal : 8.0 - 12.0 um');
  readln(IRband);
  writeln; writeln('Enter Johnson cycle criteria:');
  writeln('        A. Detection');      { potential military interest }
  writeln('        B. Classification'); { warship vs. merchant }
  writeln('        C. Recognition');    { destroyer vs. Cruiser }
  writeln('        D. Identification'); { Kashin vs. Spruance }
  readln(JohnCrit);
  writeln; writeln('Please enter the FOV: '); { MRT data given in the  }
  writeln('          A. Narrow');             { narrow FOV .. InvRatio }
  writeln('          B. Wide');               { allows calculations    }
  readln(FOV);                                { for Wide FOV           }
  case FOV of 'B','b' : begin
                          writeln('Enter Wide to Narrow FOV #');
                          readln(Wide2Narrow);
                        end;
        end;
end;

{ ************************************************************** }

procedure CalcTransmissivity (SlantRng : real; var TotTrans : real );
                                                    { calculate Transmittance from }
                                                    { humidity,range,and visibility}
  var
    Humidity,
    Wtr, Mstr,
    T_Sub_A,            { transmittance due to absorption}
    T_Sub_S,            { transmittance due to scattering}
    AlphaSub_S : real;  { extinction coefficient due to scattering }

  begin
    Humidity := 1.4 * Exp(-4.137*0.00001*Alt);  { Ave absolute humidity }
    Wtr := Humidity * SlantRng;                 { from sea level to alt }
    Mstr := 1.06 + (0.19 * Wtr) + (0.000796 * power(Wtr,2))
            + (0.000036 * power(Wtr,3))
            + (0.00000189 *power(Wtr,4));
    T_Sub_A := 1/Mstr;                          { transmittance due to absorb }
    case IRband of
```

```
            'A','a' : AlphaSub_S := 3.91/Vis;
            'B','b' : AlphaSub_S := 0.6*(3.91/Vis);  { Koschmieder Relationship }
            'C','c' : AlphaSub_S := 2.24/Vis;
            'D','d' : AlphaSub_S := 0.85/Vis;
           end;
    T_Sub_S := exp(-AlphaSub_S*SlantRng);       { transmittance due to scatter }
    TotTrans := T_Sub_A * T_Sub_S;
  end;

{  ************************************************************  }

function CalcDeltaTPrime (Trans : real) : real;

  begin
    CalcDeltaTPrime := DeltaT * Trans;
  end;

{  ************************************************************  }

procedure CalcSpatialFreq (DTPrime : real; var TargFreq : real);

  var
    InvRatio : real;
    index : integer;

  begin
    case FOV of
          'A','a' : InvRatio := 1.0;
          'B','b' : InvRatio := 1/Wide2Narrow;
         end;  { case }
    if DTPrime <= DataArray[1].Mrt then
      begin
        TargFreq := DataArray[1].Freq * InvRatio;
        write('Delta T Prime is below MINMRT of ',DataArray[1].Mrt);
        writeln(' thus cycles defaults to MINMRT cycles.');
      end
    else
      if DTPrime >= DataArray[ArraySize].Mrt then
        begin
          TargFreq := DataArray[ArraySize].Freq * InvRatio;
          write('Delta T Prime exceeded MAXMRT of ',DataArray[ArraySize].Mrt);
          writeln(' thus cycles defaults to MAXMRT cycles.');
        end
      else
        begin
          for index := 1 to (Arraysize - 1) do
            begin
              if (DataArray[index].Mrt <= DTPrime)
                and (DataArray[index+1].Mrt >= DTPrime) then
```

```
                TargFreq := LogInterp(DataArray[index].Mrt,
                        DataArray[index+1].Mrt, DTPrime,
                        DataArray[index].Freq * InvRatio,
                        DataArray[Index+1].Freq * InvRatio);
            end; { for }
        end; { else }
    end;

{ ************************************************************** }

procedure CalcCriticalDimension (Dist : real; var D_Sub_C : real);

    var
      HsubO, h,          { HsubO = obscuration by horizon }
      Horizon,           { h = actual height seen       }
      Theta,             { Horizon = function of Altitude }
      Area : extended;   { Theta = elevation angle      }
                         { Converts Degs to Rads by * Pi/180 }
    begin
      HsubO :=  0.0;
      h := 0.0;
      Theta := 0.0;
      Horizon := 1.23 * (Sqrt(Alt));
      Horizon := NmToKm(Horizon);
      if Dist >= Horizon then
        begin
          HsubO := (sqr(Dist*1000)/(2*EarthRad))
                    - ((Dist*1000)*(Sqrt((2*AltM)/EarthRad))) + AltM;
        end;
      h := Height - HsubO;
      Theta := ArcSin(AltM,Dist);
      if Azimuth = 90.0 then
        begin
          Azimuth := 89.99999;
        end;
      Area := (Length * Width * Sin(Theta*Pi/180))
            + (h * Width * Cos(Theta*Pi/180) * Sqrt(1-(power(Sin(Azimuth*Pi/180),2) *
              power(Cos(Theta*Pi/180),2))))
            + (h * Length * Cos(Theta*Pi/180) * Sqrt(1-(power(Cos(Azimuth*Pi/180),2) *
              power(Cos(Theta*Pi/180),2))));
      D_Sub_C := Sqrt(Area);
    end;

{ ************************************************************** }

function ResolvCycles (Vr : real; Dc : real; Rng : real) : real;

    var
      Denom : real;
```

```
  begin
    if Rng = 0.0 then
      begin
        Denom := AltM/1000;
        ResolvCycles := (Vr * Dc)/Denom;
      end
    else
      begin
        ResolvCycles := (Vr * Dc)/Rng;
      end;
  end;

{ ************************************************************** }

procedure FindP_inf(CycFreq : real; var Pinf : real);

  var
    Fov_50, InvMrad, exponent, num : double;

  begin
    case JohnCrit of
          'A','a' : Fov_50 := 0.75;
          'B','b' : Fov_50 := 1.5;
          'C','c' : Fov_50 := 3.0;    { Johnson Criteria }
          'D','d' : Fov_50 := 6.0;
        end;   { case }
    InvMrad := CycFreq/Fov_50;
    exponent := 2.7 + (0.7 * InvMrad);
    num := power(InvMrad, exponent);
    Pinf := num/(1 + num);
  end;

{ ************************************************************** }

procedure Output;

  var
    index : integer;
    Pstar, value : real;
  begin
    clrscr;
    writeln('          ****************************************');
    writeln('             OUTPUT DYNAMIC FLIR PROBABILITY');
    writeln('          ****************************************');
    writeln; writeln; writeln;
    writeln('For the following inputs:');
    writeln;
    writeln('Target size(m) of: ',Length:5:2,' x ',Width:5:2,' x ',Height:5:2);
    writeln('Altitude:  ',Alt:5:0,' FEET');
```

```
    writeln('Azimuth:  ',Azimuth:3:0,' DEGREES');
    writeln('Delte T:  ',DeltaT:4:2,' DEGREES CELCIUS');
    writeln;
    case FOV of
          'A','a' : begin
                      writeln('NARROW FOV:');
                    end;
          'B','b' : begin
                      writeln('WIDE FOV:');
                    end;
        end;  { case }
    writeln;
    case JohnCrit of
          'A','a' : begin
                      writeln('Probability of DETECTION:');
                    end;
          'B','b' : begin
                      writeln('Probability of CLASSIFICATION:');
                    end;
          'C','c' : begin
                      writeln('Probability of RECOGNITION:');
                    end;
          'D','d' : begin
                      writeln('Probability of IDENTIFICATION:');
                    end;
        end;  { case }
    writeln; writeln;
    writeln('PROB    RANGE(Km)');
    Pstar := 0.95;
    while Pstar >= 0.04 do
      begin
        for index := 0 to (RngInc - 1) do
          begin
            if (ProbArray[index].Prob >= Pstar)
              and (ProbArray[index+1].Prob <= Pstar) then
                begin
                  value := LogInterp(ProbArray[index].Prob,
                        ProbArray[index+1].Prob, Pstar,
                        ProbArray[index].Rng,
                        ProbArray[index+1].Rng);
                 { value := KmToNm(value);     +++ To output NM+++}
                  writeln(Pstar:3:2,'      ',value:5:3);
                  end;  { if }
          end;  { for }
        Pstar := Pstar - 0.05;
      end;  { while }
  end;

{  ************************************************************  }
```

```
BEGIN
  assign (Infile,'A:\flir.in');
  assign (Probfile,'a:\flir.prb');
  repeat
    reset(Infile);
    rewrite(Probfile);
    Initialize;
    GetData;
    RngInc := round (Alt / 3280);
    if RngInc > Range then
      begin
        write('Range Not Long Enough ... Run Again With a ');
        writeln('LONGER INITIAL RANGE !');
      end;
    if RngInc < 1 then RngInc := 1;
    while (RngInc <= Range) and (ProbArray[RngInc - 1].Prob >= 0.05) do
      begin
        CalcTransmissivity(RngInc,Trnsmiss);
        DeltaTPrime := CalcDeltaTPrime(Trnsmiss);
        CalcSpatialFreq(DeltaTPrime,VsubR);
        CalcCriticalDimension(RngInc,CritDem);
         Cycles := ResolvCycles(VsubR, CritDem, RngInc);
        FindP_Inf(Cycles, Prob);
        ProbArray[RngInc].Rng := RngInc;
        ProbArray[RngInc].Prob := Prob;
        if RngInc >= (MaxArraySize - 10) then  { warning to user }
          begin
            writeln('Approaching Array Limit');
            writeln('Press any key to continue.....');
            RunFlag := readkey;
          end;
        inc(RngInc);
      end;
      Output;
      writeln('Do you want to RUN AGAIN ?  (Y/N) ');
      readln(RunFlag);
    until (RunFlag = 'N') or (RunFlag = 'n');
   close(Infile);
   close(Probfile);
   writeln; writeln('This concludes the Program!!!!!!');

END.
```

APPENDIX B. TARGET AREA FORMULA DERIVATION

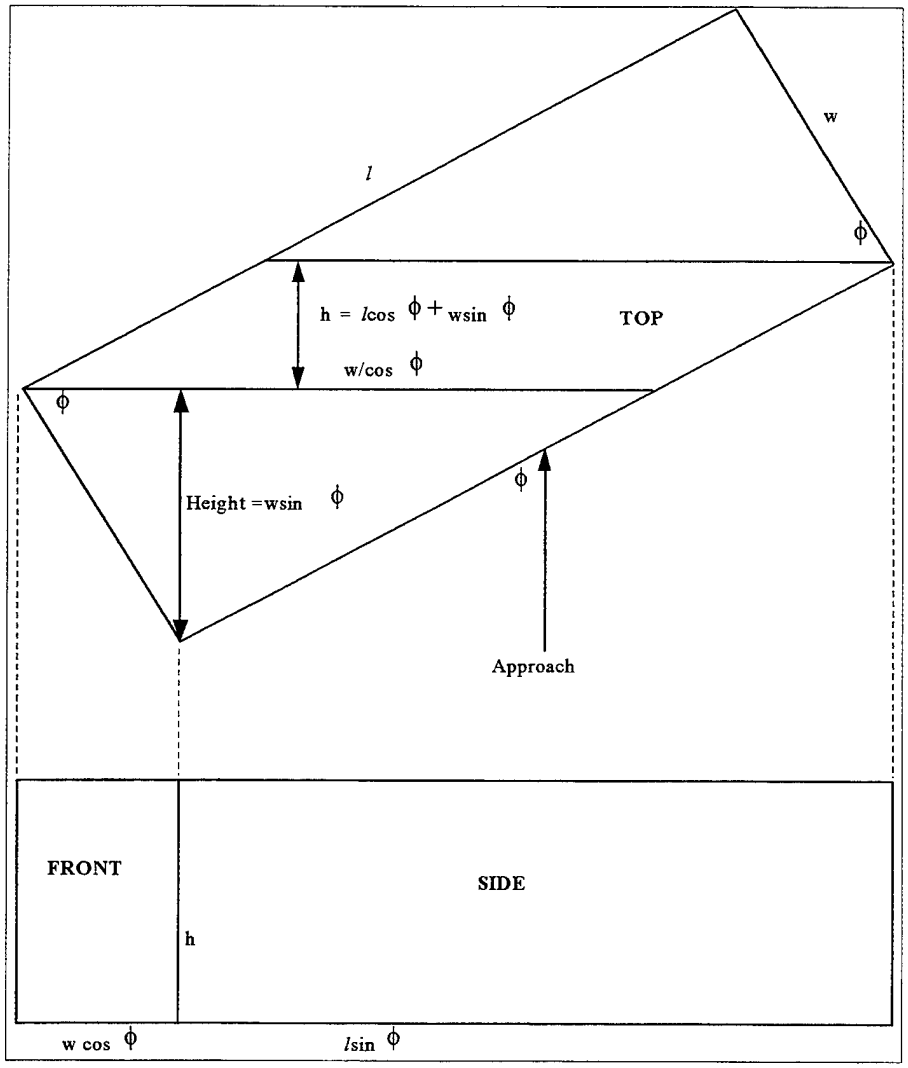

Figure B.1: Vertical and Horizontal Views of an Object.

Area of Top "Seen":

When directly overhead (i.e., $\theta = 90°$) the area seen is independent of the horizontal approach angle ϕ; the top area seen is that in the upper diagram of Figure B.1, namely lw.

If the object is approached from a horizontal angle ϕ and a vertical angle of $\theta < 90°$, each triangle in the upper diagram of Figure B.1 has area $= \frac{(w/\cos\phi)(w\sin\theta)}{2}$ and the parallelogram has area $= \left(\frac{w}{\cos\phi}\right)(l\cos\phi + w\sin\phi)(\sin\theta)$. Thus the top area seen simplifies to $l w \sin\theta$.

Area of Side "Seen":

When looking horizontally (i.e., $\theta = 0°$) the area seen depends on the horizontal approach angle ϕ and is equal to $h l \sin\phi$ as shown in the lower diagram of Figure B.1. If the object is approached from a vertical angle of $\theta < 90°$ and a horizontal angle ϕ, the height seen is $h\cos\theta$, and the length seen is $\sqrt{(l\cos\phi\sin\theta)^2 + (l\sin\phi)^2}$ which simplifies to: $l\sqrt{(1 - \cos^2\phi\cos^2\theta)}$. Thus the side area seen is $hl\cos\theta\sqrt{(1 - \cos^2\phi\cos^2\theta)}$.

Area of Front/Stern "Seen":

Using similar arguments to those in the above paragraph, it can be shown that the front/stern area seen is given by: $hw\cos\theta\sqrt{(1 - \sin^2\phi\cos^2\theta)}$.

Total Area of Object "Seen" :

The total area seen is then given by:

$$A_T = lw\sin\theta + hw\cos\theta\sqrt{(1 - \sin^2\phi\cos^2\theta)} + hl\cos\theta\sqrt{(1 - \cos^2\phi\cos^2\theta)}.$$

This is Equation 3.8 on page 21 of the thesis.

LIST OF REFERENCES

1. Lloyd, J. M., *Thermal Imaging Systems*, Plenum Press, 1975.

2. Koc, C., *Modeling and Experimental Testing For Future Development of Night Vision Electro-Optic (NVEO) FLIR92 Model*, Masters Thesis in Systems Engineering, Naval Postgraduate School, Monterey, CA, December, 1995.

3. U.S. Army Night Vision and Electronic Sensors Directorate, *ACQUIRE Range Performance Model for Target Acquisition Systems*, User's Guide, May 1995.

4. Waldman, G., and Wootton, J., *Electro-Optical Systems Performance Modeling*, Artech House, Inc., 1993.

5. Shumaker, D. L., Wood, J. T., and Thacker, C. R., *Infrared Imaging Systems Analysis*, Environmental Research Institute of Michigan, 1993.

6. Hudson, R. D., *Infrared System Engineering*, John Wiley and Sons, Inc., 1969.

7. Kreitz, J. C., *Preliminary Evaluation of the PREOS Program for Determining Detection Ranges of Airborne FLIR Systems*, Masters Thesis in Physics, Naval Postgraduate School, Monterey, CA, December 1992.

8. Burnay, S. G., Williams, T. L., and Jones, C. H., *Applications of Thermal Imaging*, Adam Hilger Inc., 1988.

9. Dodson, R. G., *A Comparison of FLIR Performance Prediction Models : UFLIR and MKII TDA*, Masters Thesis in Systems Engineering, Naval Postgraduate School, Monterey, CA, September 1989.

10. Accetta, J. S., and Shumaker, D. L., *The Infrared and Electro-Optical Systems Handbook, Volumes I - VIII*, Environmental Research Institute of Michigan and SPIE Optical Engineering Press, 1993.

11. CECOM Center for Night Vision & Electro-Optics, Report R5008986, *C2NVEO Thermal Imaging Systems Performance Model*, August 1990.

12. Eadon, E., *Microcomputer Techniques for Comparing Weapons System's Target Acquisition Capabilities*, Directorate for Theater Force Analysis Technical Paper P-2022, June 1987.

13. Wolfe, W. L., and Zissis, G. J., *The Infrared Handbook*, Environmental Research Institute of Michigan, 1978.

INITIAL DISTRIBUTION LIST

		No. Of Copies
1.	Defense Technical Information Center 8725 John J. Kingman Rd., STE 0944 Ft. Belvoir, Virginia 22060-6218	2
2.	Dudley Knox Library Naval Postgraduate School 411 Dyer Rd. Monterey, California 93943-5101	2
3.	Professor Kneale T. Marshall, Code OR/Mt Naval Postgraduate School Monterey, California 93943	4
4.	Professor Gordon Bradley, Code OR/Bz Naval Postgraduate School Monterey, California 93943	1
5.	Professor W. K. Krebs, Code OR/Kw Naval Postgraduate School Monterey, California 93943	1
6.	Professor Alfred W. Cooper, Code PH/CR Naval Postgraduate School Monterey, California 93943	1
7.	Lockheed Martin Electronics and Missiles Attn: Jane Johns 5600 Sand Lake Rd. MP-457 Orlando, Florida 32819-8907	2
8.	LT. Jeffery P. Eaton 502 Bonita Dr. Lady Lake, Florida 32159	2